

ANALYSIS OF TEXTILE COMPOSITE STRUCTURES WITH FINITE VOLUME-P-ELEMENTS

*L. Aschenbrenner*¹, *D. Hartung*¹, *J. Teßmer*¹

¹*Institute of Composite Structures and Adaptive Systems, Dep. of Structural Analysis German Aerospace Center (DLR), Lilienthalplatz 7, D-38108 Braunschweig, Germany. E-mail: Lars.Aschenbrenner@dlr.de*

Abstract

The paper presents a three-dimensional finite p-element based on hierarchical shape functions. Providing anisotropic ansatz-spaces this element enables the accurate computation of three-dimensional stress states of orthotropic materials, actually of reinforced textile composites-materials. Finite element analysis of a thick walled mounting plate of an elevator bucket is demonstrated whereas the spatial discretisation error is indicated by a posteriori error estimation. Failure of the textile composite is predicted by a criterion that was developed for three-dimensional reinforced laminates. Necessary through-the-thickness material properties and parameters are determined based on experimental results utilising a new modified Arcan testing device. This device enables testing under combined out-of-plane load conditions.

1. Introduction

Anisotropic textile composites show complex deformation and failure behaviour. In particular three-dimensional reinforced textile composites are characterised by an orthotropic material behaviour. To achieve the full potential of textile composites the material and especially the 3d failure behaviour has to be analysed. Particularly regions dominated by three-dimensional stress states, e. g. load introduction areas have to be explored in more detail. In such areas or thick structures proper computation of three-dimensional stress distributions requires the use of volume elements because shell theories come to their limits of validity. Especially for the purposes of analysing thick composite structures a volume element based on hierarchical shape functions is being developed, [7]. Additionally in our work the element is used within the p-version of the finite element method to achieve superior convergence properties during the computation process. Thereby different a posteriori error estimators are applied to control the spatial adaptivity of polynomial order of the shape functions. In case of the selected anisotropic ansatz space for the displacements even a simple error indicator is able to distinguish between the error contribution of in- and out-of-plane stresses.

In applications used material parameters to describe the deformation and failure behaviour of textile laminates are based on experimental investigations. With focus on out-of-plane properties a modified version of a test device commonly known as the Arcan test was developed. The material behaviour of Carbon and E-Glass Non Crimp Fabrics (NCF) composites were experimentally explored. The performance of composites materials under combined through-the-thickness stress σ_{zz} with interlaminar shear stresses τ_{xz} , τ_{yz} are experimentally analysed. The numerical model and the determined parameters are validated by finite element simulations of the conducted Arcan tests. Applicability of the developed finite p-element implementation is demonstrated by analysis of a mounting plate of an elevator bucket. Thereby the mounting plate is modelled as a substructure coupled to the global model by prescribed displacements. The model shows a pronounced three-dimensional stress state for that failure is predicted caused by the out-of-plane stresses.

2. Volume p-element formulation

Finite element formulations can be associated to the h- or p-method due to how convergence of the numerical solution is achieved. H-method achieves convergence by mesh refinements while the polynomial degree of the ansatz remains constant. In contrast in p-method the mesh remains unchanged and convergence is assured by increasing the polynomial degree of the shape functions. Investigations during the past 20 years [4, 5, 10] have shown that hierarchical shape function have superior characteristics compared to standard shape functions based on Lagrange polynomials.

The developed element interpolates the displacements by sets of higher order hierarchical shape functions derived from Legendre polynomials. This shape functions are orthogonal. Thus round-off errors usually associated with polynomials of high degree are avoided. Coupling between hierarchical degrees of freedom is minimized and a more dominant diagonal form of the stiffness matrix is obtained. This ensures an improved condition of the stiffness matrix.

2.1. Hierarchical shape functions

Shape functions are called hierarchical if the basis functions of degree p are embedded in the set of shape functions of degree $p + 1$, thereby all shape functions have to be orthogonal. Figure 1 displays a set of hierarchical shape function for the two-dimensional case based on linear interpolation and the polynomials $\Phi_n(x)$ defined by equation (1).

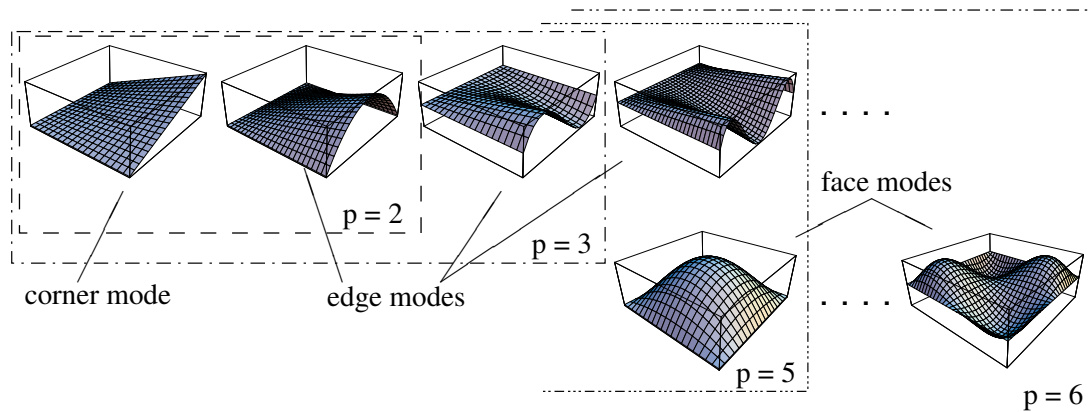


Fig. 1. Sets of hierarchical shape functions in 2 D

Within the hierarchical concept there are two different types of ansatz spaces: the isotropic space S_{3D}^p and the anisotropic space $S_{3D}^{p,q}$ used for the developed 3D composite element. The polynomial degree p for the isotropic space is the same in all local directions ξ , η and ζ . Especially the selected anisotropic space is aligned to layered composite materials. Thereby all shape functions in ξ and η direction are associated with the polynomial degree p while in $zeta$ direction the value q defines the degree of all shape functions (see figure 2 and figure 3).

The formulation of the 3d p-element uses the orthogonal normalized integrals of the Legendre polynomials $P_i(t)$:

$$\Phi_n(x) = \sqrt{\frac{2n-1}{2}} \int_{-1}^x P_{n-1}(t) dt \tag{1}$$

possessing the properties

$$(\Phi_i, \Phi_j) = \delta_{ij} \quad \text{and} \quad \Phi_n(\pm 1) = 0 \quad .$$

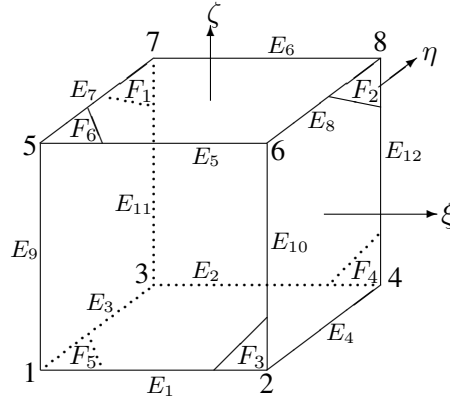


Fig. 2. Definition of nodes, edges and faces of the 3D p-element

The first four Legendre polynomials and integrated polynomials follow to:

$$\begin{aligned}
 P_0(x) &= 1 \\
 P_1(x) &= x \\
 P_2(x) &= \frac{1}{2}(3x^2 - 1) & \Phi_2(x) &= \frac{1}{2}\sqrt{\frac{3}{2}}(x^2 - 1) \\
 P_3(x) &= \frac{1}{2}(5x^3 - 3x) & \Phi_3(x) &= \frac{1}{2}\sqrt{\frac{5}{2}}(x^3 - x) \\
 P_4(x) &= \frac{1}{8}(35x^4 - 30x^2 + 3) & \Phi_4(x) &= \frac{1}{8}\sqrt{\frac{7}{2}}(5x^4 - 6x^2 + 1) \quad .
 \end{aligned}$$

Since the three-dimensional shape functions for volume elements (see figure 2) correspond to nodes, edges, faces and bodies they can be classified into four groups presented here for the anisotropic space $S_{3D}^{p,q}$.

- *Nodal shape functions (Nodal Modes)*

The linear volume element exhibits eight nodal shape functions, that are the same as in h-version concepts and the isotropic space derived from linear interpolation e. g. for the first two nodes

$$\begin{aligned}
 {}^N N^{(1)}(\xi, \eta, \zeta) &= \frac{1}{8} (1 - \xi) (1 - \eta) (1 - \zeta) \\
 {}^N N^{(2)}(\xi, \eta, \zeta) &= \frac{1}{8} (1 + \xi) (1 - \eta) (1 - \zeta)
 \end{aligned} \quad (2)$$

- *Edge Modes*

There are eight edges in-plane (E_1 bis E_8) and four out-of-plane (E_9 bis E_{12}). Thus $8(p-1)+4(q-1)$ edge modes exist. For example the shape functions of edges 1, 2, 5 and 12 are defined as

$$\begin{aligned}
 {}^E N_i^{(1)}(\xi, \eta, \zeta) &= \frac{1}{4} \Phi_i(\xi) (1 - \eta)(1 - \zeta) \quad , \quad i = 2, \dots, p \quad , \\
 {}^E N_i^{(2)}(\xi, \eta, \zeta) &= \frac{1}{4} \Phi_i(\xi) (1 + \eta)(1 - \zeta) \quad , \quad i = 2, \dots, p \quad , \\
 {}^E N_i^{(5)}(\xi, \eta, \zeta) &= \frac{1}{4} (1 - \xi) \Phi_i(\eta) (1 - \zeta) \quad , \quad i = 2, \dots, p \quad , \\
 {}^E N_i^{(12)}(\xi, \eta, \zeta) &= \frac{1}{4} (1 + \xi)(1 + \eta) \Phi_i(\zeta) \quad , \quad i = 2, \dots, q \quad .
 \end{aligned} \quad (3)$$

- *Face Modes*

The volume element exhibits 2 in-plane faces (F_5 und F_6) and 4 out-of-plane faces (F_1 bis F_4). Thus there exist $(p-2)(p-3)+4(p-1)(q-1)$ face modes. Modes of face 1, 4 and 6 are defined by

$$\begin{aligned} {}^F N_{i,j}^{(1)}(\xi, \eta, \zeta) &= \frac{1}{2}(1 - \xi) \Phi_i(\eta) \Phi_j(\zeta) \quad , \quad i = 2, \dots, p; j = 2, \dots, q \quad , \\ {}^F N_{i,j}^{(4)}(\xi, \eta, \zeta) &= \frac{1}{2} \Phi_i(\xi) (1 + \eta) \Phi_j(\zeta) \quad , \quad i = 2, \dots, p; j = 2, \dots, q \quad , \\ {}^F N_{i,j}^{(6)}(\xi, \eta, \zeta) &= \frac{1}{2} \Phi_i(\xi) \Phi_j(\eta) (1 + \zeta) \quad \begin{cases} i, j = 2, \dots, p-2 \\ i+j = 4, \dots, p \end{cases} \quad . \end{aligned} \quad (4)$$

- *Internal Modes*

The space $S_{3D}^{p,q}$ has $(p-3)(p-2)(q-1)/2$ internal modes

$${}^I N_{i,j,k}(\xi, \eta, \zeta) = \Phi_i(\xi) \Phi_j(\eta) \Phi_k(\zeta) \quad (5)$$

where

$$i, j = 2, \dots, p-2; i+j = 4, \dots, p; k = 2, \dots, q \quad .$$

2.2. Element equations

The hierarchic volume p-element formulation is displacement based. Thereby the displacement \mathbf{u} is interpolated by the linear nodal shape functions \mathbf{N}_i ($i = 1, \dots, 8$) and the hierarchical shape functions \mathbf{N}_j ($j = 9, \dots, \hat{n}$)

$$\mathbf{u} = \mathbf{N}_i \mathbf{u}_i + \mathbf{N}_j \mathbf{a}_j \quad (6)$$

where \mathbf{u}_i are nodal displacements and \mathbf{a}_j the hierarchical displacement variables. The element equation is derived in the standard way by using the principle of virtual work ending with a general iterative incremental form holding for the time $t + \Delta t$

$$\begin{aligned} \int_{V_e} \hat{\mathbf{B}}^T \cdot \mathbb{C}^k \Big|_{t+\Delta t} \cdot \hat{\mathbf{B}} \, dV_e \, d\Delta \hat{\mathbf{u}}^k = \\ \int_{V_e} \hat{\mathbf{N}}^T \cdot \mathbf{f}_{t+\Delta t} \, dV_e + \int_{A_e} \hat{\mathbf{N}}^T \cdot \mathbf{t}_{t+\Delta t} \, dA_e - \int_{V_e} \hat{\mathbf{B}}^T \cdot \boldsymbol{\sigma}^k \, dV_e \end{aligned} \quad (7)$$

where k denotes the iteration counter, $\hat{\mathbf{N}}$ the matrix of shape functions, $\hat{\mathbf{B}}$ the strain-displacement-matrix, \mathbf{f} body forces, \mathbf{t} surface tractions and $\boldsymbol{\sigma}$ the stress tensor. Unknowns of this form are the incremental displacements $\Delta \hat{\mathbf{u}}$, the iterative improved solution follows to $\Delta \hat{\mathbf{u}}^{k+1} = \Delta \hat{\mathbf{u}}^k + d\Delta \hat{\mathbf{u}}^k$. Equation (7) doesn't specify the used material model. Arbitrary models may be included into the element formulation while from the set of constitutive equations a material operator $\mathbb{C} = \frac{\partial \boldsymbol{\sigma}}{\partial \boldsymbol{\epsilon}}$ (tangential stiffness) has to be computed. Actually a linear strain displacement relation is assumed. The element stiffness matrix is integrated by Gaussian quadrature.

2.3. Implementation

The introduction to hierarchical ansatz spaces clarifies, that the total number of degrees of freedom (dof) in an element depends on the actual order of (p, q) . For the numerical implementation of this variability two concepts seems to be reasonable:

- the number of dof in an element is directly coupled with the total number of nodes,
- the number of nodes is constant causing a variable number of dof associated with nodes (nodes in sense of geometrical places).

It was followed the latter concept to implement the element formulation into the open finite element environment B2000++ provided by the swiss Company SMR. Advantage thereby is a geometrical description of the elements that is independent of the polynomial orders p, q so that pre- and postprocessing are equivalent to cubic standard elements. Generally this concept requires a FE-program-kernel allowing for an at runtime adjustable (dynamical) element formulation. Figure 3 displays as an example the distribution of dof for the ansatz space $S_{3D}^{2,3}$. To all nodes of out-of-plane edges six dof are assigned, all other nodes are allocated by three dof's.

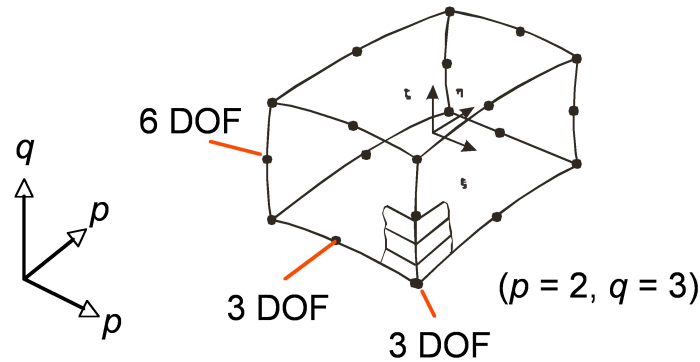


Fig. 3. p -element, number of dof's at nodes e. g. $p = 2, q = 3$

2.4. Adaptive modelling and error estimation

Goal of adaptive modelling strategies in FEA is to achieve a more efficient and accurate solution of the given mechanical problem. Normally adaption of the discretisation (the ansatz space) and steering of the solution algorithm respectively are successful methods. Basis of steering h- or p-adaptivity in FEA is error estimation. In Literatur it is differentiated between error indication and estimation whether qualitative predictions or quantitative bounds of the error are given. Further informations and explanantions are given in detail by [1]. Reference solutions used for the error estimation play a very important role. But even for practical relevant problems exact solutions are in general unknown therefore mostly the error is extrapolated by the difference of two computed solutions. If the error is predicted only in dependency of mesh data and further input data one speaks of a priori estimation. Estimation utilising the already computed solution is called a posteriori estimation. Actually a posteriori estimators of the following two general groups are implemented within the volume p-element code:

1. Indication based on gradient recovery

Basic idea is the introduction of averaged continuous stresses $\sigma_{average}$. The L^2 -norm of the difference between $\sigma_{average}$ and the approximated discontinuous stress σ_h

$$\|\sigma_h - \sigma_{average}\| \rightarrow \min \quad (8)$$

is an indicator of the dominating error. Great advantage of these estimators/indicators is the low computational effort. The most important disadvantage is that no real bounds of the error are given. Important candidates of these indicators are presented in [9, 11, 12]

2. Element residual methods

Starting point is the main equation of error analysis, [1]. These estimators take the element residuum

$$\mathbf{R} := \operatorname{div} \sigma_h + \mathbf{f}$$

and the stress discontinuities on the element boundaries

$$\mathbf{J} := \begin{cases} \frac{1}{2}(\boldsymbol{\sigma}_h^+ \mathbf{n}^+ + \mathbf{n}^- \boldsymbol{\sigma}_h^-) & \text{on } \partial K_i \\ \mathbf{t} - \boldsymbol{\sigma}_h \mathbf{n} & \text{auf } \partial K_N \\ \mathbf{0} & \text{on } \partial K_D \end{cases}$$

as a measure for the element error into account. The error $\mathbf{e} = \mathbf{u} - \mathbf{u}_h$ could be estimated in the energy norm with help of the CHAUCHY-SCHWARZ-inequality to

$$\|\mathbf{e}\|^2 \leq C \bigcup_{(K)} \left\{ h_K^2 \|\mathbf{R}\|_{L_2(K)}^2 + h_K \|\mathbf{J}\|_{L_2 \partial K}^2 \right\} \quad \text{with} \quad \|\dots\|_{L_2(K)}^2 = \left(\int_{\Omega} |\dots|^2 dV \right)^{\frac{1}{2}}$$

thereby the constant C couldn't be determined in general. For example Babuška and Rheinboldt proposed such an estimator, [3].

An error indicator of the gradient recovery type was selected because of its simplicity and the low computational costs. The indicator is enhanced and modified in form of different weightings of stress components and normalisation to global maximum stress values before evaluating equation (8). This indicator is then able to serve nodal information about spatial directions in which deficiencies of the ansatz space lead to high contributions to the error of the stress-field. Thus this indicator gives reasonable results to adopt the polynomial orders p and q . To get a measure of the overall error and get information about the element wise error contributions a residual error estimator is evaluated too. As an example figure 7 visualises the residual error measures as vectors on element faces and in the element volume in order to give an idea about the spatial distribution.

3. Through-the-thickness tests

3.1. Test device

The most important requirement for the experimental determination of out-of-plane properties was the applicability in a standard hydraulic test machine. Therefore a test device for tubular specimens was not useable. Only uniaxial movement of the test equipment was available even though combined load conditions should also be feasible. For all experiments an Instron 100 kN hydraulic test machine was used.

A promising concept to test composites under combined shear and tensile load conditions was originally published 1977 by ARCAN ET AL. [2]. In our application a modified Arcan test rig is used. The specimen is installed in the test rig as displayed in figure 4 (a). The waisted specimen (pos. 9) is installed in the centre of the disk with a specimen inset (pos. 4). That allows quick installations of different specimens by changing complete insets with already installed specimens. The specimen inset is mounted by adjustable clamping devices (pos. 2). The position of the disks can be changed in seven steps from pure tensile trough to pure shear and combined tensile shear load conditions. Fits are used to adjust the precise orientation thereby each half of disk is clamped with 4 screws. Two identical halves of disks are used on the front and back side. To enable quicker installation of different specimens a modular specimen inset was developed. Specimens are installed in a centre plate which is clamped by screws on two outer plates. Therefore only the specimen within the centre plate has to be changed. The specimen is bonded to the centre plate with an adhesive (X60). The metallic parts are pre-treated with releasing agent. The two component adhesive bonding is low viscous and the experience has shown that the manufacturing tolerances between the specimen and the cut out of the centre plate are best filled with a fast curing adhesive. For that purpose an aligned bonding fixture is used to guarantee a precise specimen orientation. Therefore a widely unproblematic specimen installation is feasible.

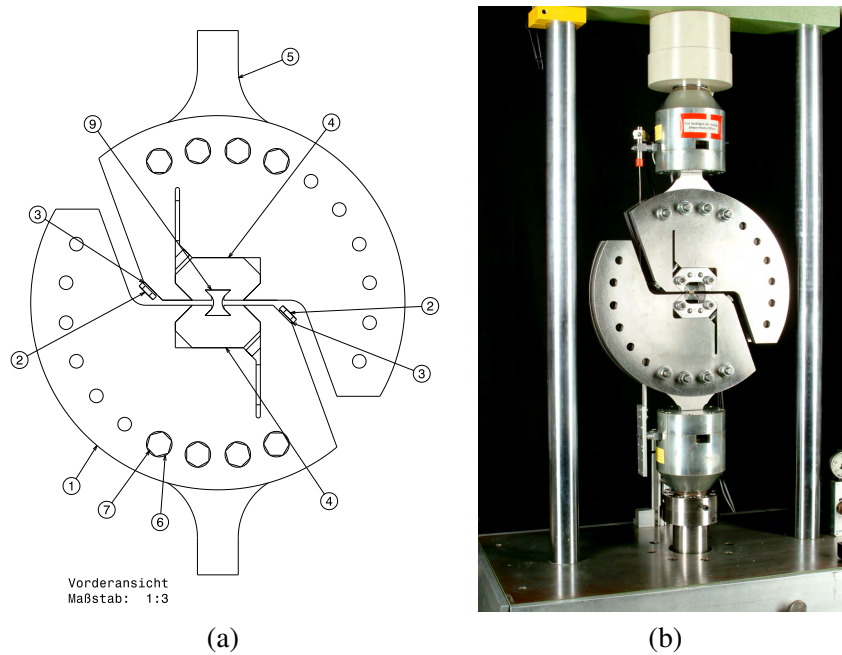


Fig. 4. a) Modified Arcan Device b) Installation in uniaxial Instron test machine

3.2. Test Results

A choice of Carbon and E-Glass fibre composites are tested. Both materials are untufted Non Crimp Fabrics (NCF). All specimens fail within the waisted cross section like shown by figure 5. The material deformations are typically measured by a double strain gauge for the vertical and horizontal direction on the specimen front and if required with a single strain gauge for the transversal contraction on one side of the specimens. For future tests a strain gauge rosette will be used to measure the full deformation of the specimen.

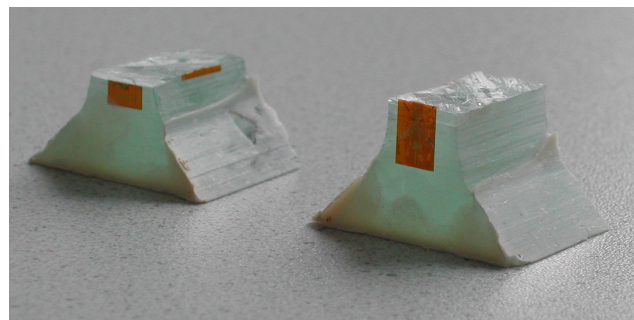


Fig. 5. Failed NCF E-Glass tensile specimen

A direct connection of the polyester stitching yarn of the NCF preform to the failure behaviour of the E-Glass as well as Carbon materials could not be determined. The failure surface and failure behaviour under through-the-thickness load conditions seems to be independent to the influence of the Polyester stitching yarn.

3.3. Quasi-isotropic NCF E-Glass specimen

The material behaviour of E-Glass fibre composites is mostly ductile compared with Carbon fibre composites. This results in higher material compliances and cause problems by testing the out-of-plane behaviour. The test results on the left in figure 6 of quasi-isotropic E-Glass NCF

composites under through-the-thickness tensile loading is accompanied by a form of stuck and sliding process. This phenomenon was not measurable with Carbon composites and seems to be the consequence of higher material compliances of E-Glass composites. In consequence that the specimens are not rigidly clamped they can slip locally and partially reducing local stresses. This behaviour appears in the stress strain curve as a horizontal jump backwards. Therefore these effects are probably the consequence of the load transfer through the inset wedges and correspond with the material compliances within a local region of the specimen. Nevertheless nearly the same elasticity modulus is measured between each sliding effect. Therefore a continuous stress strain curve as shown on the right in figure 6 is approached if the measured values after each sliding effect are added with a strain offset. These offsets correspond to the sliding distance during the test. By continuously loading the material failure is reached within the waisted cross section of the specimen and the conditions due to the wedge introduced test load are not characteristic for the final material failure behaviour.

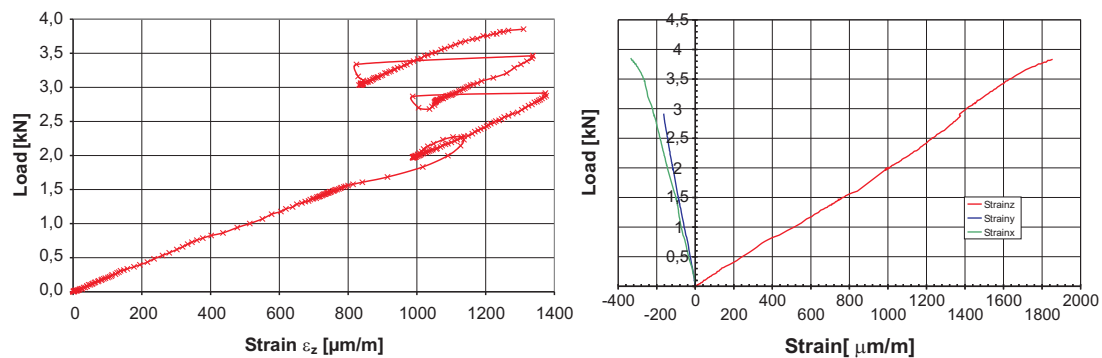


Fig. 6. Tensile load strain curve and modified load strain curve for E-Glass specimen

4. Numerical Simulations

4.1. FE simulation of out-of-plane experiments in Arcan test device

For verification purposes of the applied failure criterion finite element simulations of the modified Arcan test were conducted. The parameter set of the failure criterion is determined by multi scale analysis as proposed in [8] because some of the parameters don't admit an direct experimental determination. Figure 7 depicts the displacement field strongly amplified due to the prescribed displacement of the lower fixtures. For the selected finite element mesh the discretisation error was evaluated by a posteriori estimation of residual errors. On the right Figure 7 shows the error measure as vectors on element surfaces and in the element volume. The visualisation makes clear that a considerable error only occurs in the region of the transition from the fixtures to the waisted cross section. This error decays very rapidly so that there is no influence on the stress state within the mainly tested cross section.

In case of the numerical failure analysis of the E-Glass NCF first a displacement of 0,001 mm at the lower fixtures was preset. For each sublayer of the E-Glass NCF the failure criterion of JUHASZ [6] was evaluated for a set of selected points. Elements in the region of the waisted cross section incorporate 8 sublayers of the E-Glass laminate. Figure 8 displays on the left the predicted margin of safety at each point of all sublayers. As expected the minimal margins appear at the flanks where the cross section has its minimal area, plotted in dark blue. For the lowest value of 112.21 the maximum stress component σ_{zz} causing fracture in x-y-plane follows to 49.4 MPa. This value is in good accordance with experimental results, there strength values in thickness direction between 42.0 and 51.8 MPa were measured. Figure 8 presents on

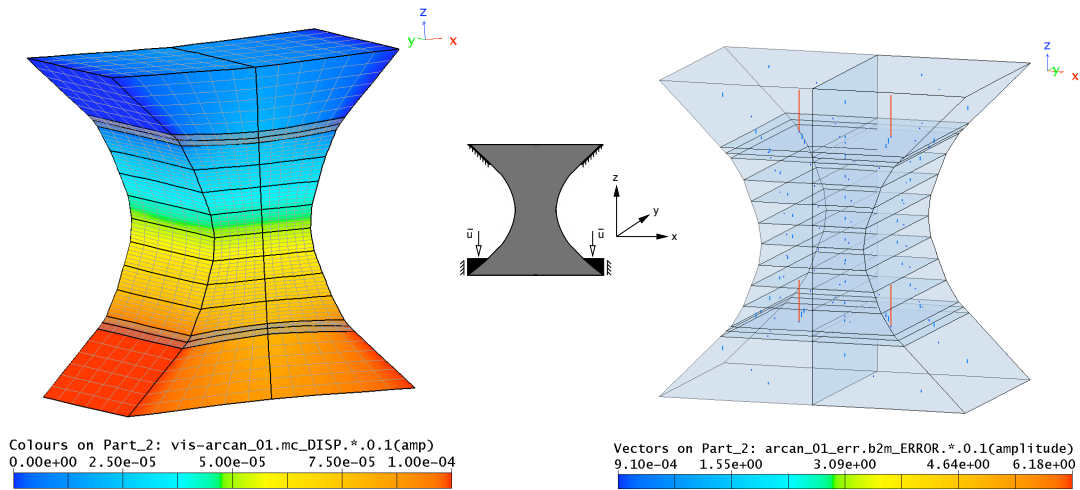


Fig. 7. Displacement field and residual error of the volume and the faces

the right for each sublayer the stress distribution of the z-component. Except for the border areas the stress distribution is homogeneous within the waisted cross section as required during specimen design. Stress peaks occur only localised at specific points near the free edges at the waisted flanks. Due to the load introduction the upper and lower fixtures cause a small area of compression in z-direction near the edges.

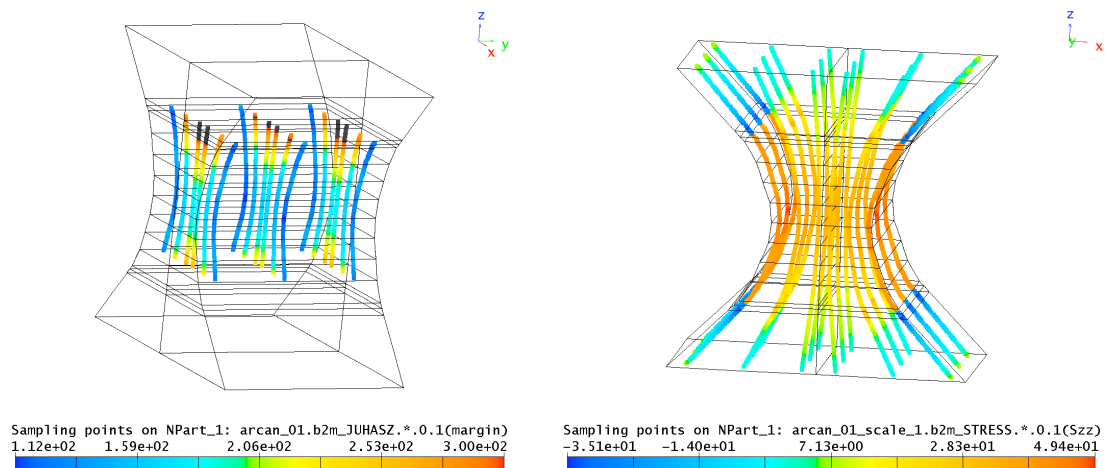


Fig. 8. Margin of safety for sublayers of E-Glass NCF and stress component σ_{zz} at failure

4.2. Analysis of a mounting plate of an loading elevator bucket

At the load introduction of an loading elevator bucket like displayed in figure 9 the structural thickness is large against the other dimensions so that for numerical analysis a discretisation with volume elements is required.

In the presented simulations the mounting plate is analysed as a substructure of the global shell model coupled through prescribed boundary conditions of the nodal displacements. Figure 9 shows a sketch of the mechanical system, the holes are totally fixed. In the submodel one p-element incorporates about 40 sublayers of the E-Glass laminate. On the right of figure 9 the displacement field caused by the prescribed boundary conditions is visualised. Evaluation of the residual errors analogue to section 4.1. has shown that satisfactory approximations of the displacements and stresses with the quite coarse mesh need polynomial orders of the shape

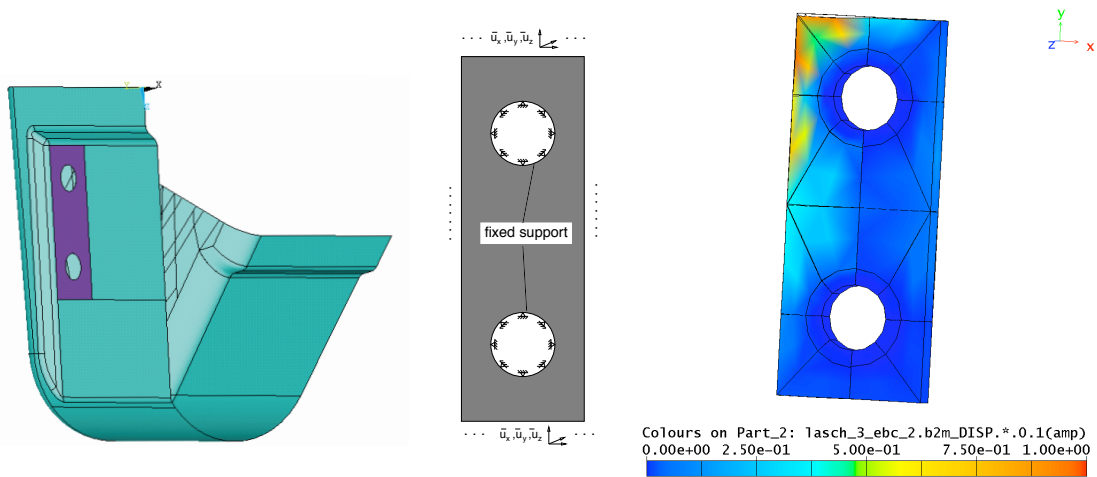


Fig. 9. Loading elevator bucket, mechanical system of the substructure, displacement amplitude

functions above five. The global displacement field is in total relative smooth. For the given load case of prescribed boundary conditions the failure criterion of JUHASZ [6] considering the validated parameters was applied for selected points in x-y-plane for each sub-layer.

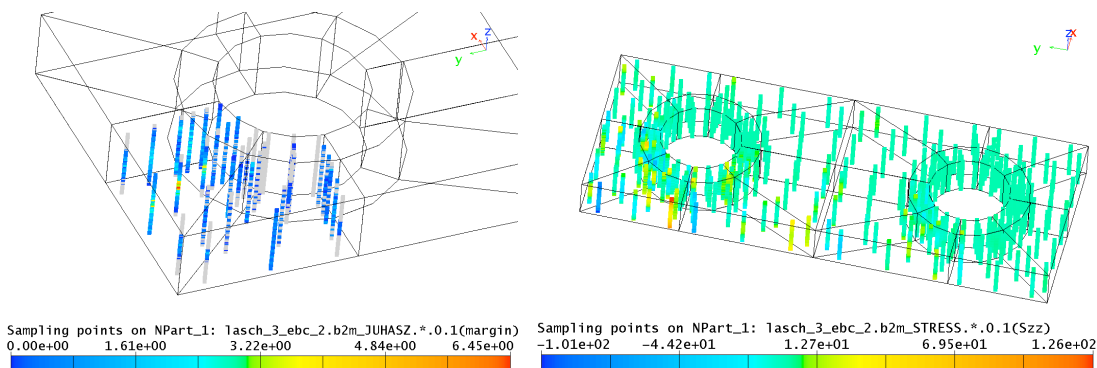


Fig. 10. Margin of safety and stress σ_{zz} for each sublayer of the E-Glass NCF

Figure 10 displays the margin of safety for each sublayer with a zoom to the upper left corner of the mounting plate. According to the applied failure criterion material strength is in many cases exceeded plotted as grey points especially near the hole. Regarding the stress distribution of the component in thickness direction in figure 10 it becomes apparent that the experimentally determined through thickness strength will be exceeded due to the occurring three-dimensional stress states. Destructive experiments of the first elevator bucket prototypes can providing data for estimation of the load bearing capacity but weren't conducted yet so that validation on structural level will be future work.

5. Conclusions and outlook

A three-dimensional finite p-element based on hierarchical shape functions has been developed. This element enables the accurate computation of three-dimensional stress states providing an alignment of the ansatz-spaces to layered orthotropic materials like reinforced textile composites too. Within the finite element analysis of a thick walled mounting plate of an elevator

bucket failure of the textile composite was predicted by a criterion developed especially for three-dimensional reinforced laminates. Discretisation errors were computed by a posteriori error estimation to adopt the polynomial order of the implemented hierarchical shape functions. Experimental results of through-the-thickness tests utilising a new modified Arcan testing device served as the basis to determine material properties and model parameters. Currently ongoing investigation concentrate on both improvements of the error estimation and enhancements of implemented material models.

6. Acknowledgments

This research was possible due to the financial support of the DFG (Deutsche Forschungsgemeinschaft). The work was partially supported by results of studies done within the I-TOOL (“Integrated Tool for Simulation of Textile Composites”) project founded by the European Commission. Furthermore the technical support and especially the improvements in visualisation given by the team of SMR (Switzerland) are gratefully acknowledged.

References

1. Ainsworth, M. and Oden, J.T., A posteriori Error Analysis in the Finite Element Analysis. *John Wiley and Sons, Inc*, 2000.
2. Arcan, M., et al., A method to produce uniform plane-stress states with applications to fiber-reinforced materials. *Experimental Mechanics* **18**: 141–146 (1977).
3. Babuška, I. and Rheinboldt, W.C., Error estimates for Adaptive Finite Element Computations. *SIAM J. Numer. Anal.* **15**: 736–754 (1978).
4. Babuška, I. Szabó, B. A. and Katz, I. N. The p-version of the finite element method. *SIAM journal on numerical analysis* **18**: 515-545 (1981).
5. Düster, A. and Rank, E. The p-version of the finite element method compared to an adaptive h-version for the deformation theory of plasticity. *Computer Methods in Applied Mechanics and Engineering* **190**: 1925-1935 (2001).
6. Juhasz, J., Rolfes R. and Rohwer K. A new strength model for application of a physically based failure criterion to orthogonal 3D fiber reinforced plastics. *Composite Science and Technology* **61**: 1821–1832 (2001).
7. Kuhlmann, G. and Rolfes, R. A hierarchic 3d finite element for laminated composites. *International Journal for Numerical Methods in Engineering* **61**: 96–116 (2004).
8. Rolfes, R., Ernst, G., Vogler, M. and Hühne, C. Material and failure models for textile composites. In *P. P. Camanho, C. G. Dávila, S. T. Pinho and J. Remmers (Eds.), Mechanical response of composites* (submitted) Springer (2007).
9. Stein, E. and Rust, W., Mesh Adaptions for Linear 2D Finite Element Discretizations in Structural Mechanics, especially in Thin Shell Analysis. *J. Comp. Appl. Math.* **36**: 107–129 (1991).
10. Szabó, B. A. and Babuška, I. Finite element analysis. *John Wiley & Sons Inc., New York* 1991
11. Zienkiewicz, O.C. and Zhu, J.Z., A simple error estimator and adaptive procedure for practical engineering analysis. *Int. J. Numer. Meth. Engrg.* **24**: 337–357 (1987).
12. Zienkiewicz, O.C. and Zhu, J.Z., The superconvergent patch recovery and a posteriori error estimates. Part 1: The recovery technique. *Int. J. Numer. Meth. Engrg.* **33**: 1331–1364 (1992)